CHACHERAU, Y., and CHANSON, H. (2011). "Bubbly Flow Measurements in Hydraulic Jumps with Small Inflow Froude Numbers." *International Journal of Multiphase Flow*, Vol. 37, No. 6, pp. 555-564 (DOI: 10.1016/j.ijmultiphaseflow.2011.03.012) (ISSN 0301-9322).

BUBBLY FLOW MEASUREMENTS IN HYDRAULIC JUMPS WITH SMALL INFLOW FROUDE NUMBERS

by Yann CHACHEREAU and Hubert CHANSON ([1])

([1]) The University of Queensland, School Civil Engineering, Brisbane QLD 4072, Australia

Fax: (61 7) 33 65 45 99 - Email: h.chanson@uq.edu.au - Url: http://www.uq.edu.au/~e2hchans/

Abstract: The transition from supercritical to subcritical open channel flow is characterised by a strong dissipative mechanism called a hydraulic jump. A hydraulic jump is turbulent and associated with the development of large-scale turbulence and air entrainment. In the present study, some new physical experiments were conducted to characterise the bubbly flow region of hydraulic jumps with relatively small Froude numbers ($2.4 < Fr_1 < 5.1$) and relatively large Reynolds numbers ($6.6 \times 10^4 < Re < 1.3 \times 10^5$). The shape of the time-averaged free surface profiles was well defined and the longitudinal profiles were in agreement with visual observations. The turbulent free-surface fluctuation profiles exhibited a peak of maximum intensity in the first half of the hydraulic jump roller, and the fluctuations exhibited some characteristic frequencies typically below 3 Hz. The air-water flow properties showed two characteristic regions: the shear layer region in the lower part of the flow and an upper free-surface region above. The air-water shear layer region was characterised by local maxima in terms of void fraction and bubble count rate. Other air-water flow characteristics were documented including the distributions of interfacial velocity and turbulence intensity. The probability distribution functions (PDF) of bubble chord time showed that the bubble chord times exhibited a broad spectrum, with a majority of bubble chord times between 0.5 and 2 ms. An analysis of the longitudinal air-water structure highlighted a significant proportion of bubbles travelling within a cluster structure.

Key words : Hydraulic jumps, Air bubble entrainment, Bubbly flow properties, Physical modelling.

INTRODUCTION

In an open channel, a high-velocity flow changes into a slower motion associated with a strong dissipative mechanism, called a hydraulic jump (Fig. 1). The hydraulic jump is an extremely turbulent flow motion characterised by the development of large-scale turbulence, energy dissipation and air entrainment. A hydraulic jump is a rapidly-varied flow and the large-scale turbulence region is called the roller. It is commonly encountered in hydraulic structures and stilling basins, storm waterways, water treatment plants and chemical processing plants. The flow within a hydraulic jump is extremely complicated (HAGER 1992, CHANSON 2009), and it remains a challenge to scientists and researchers.

A key feature of large size hydraulic jumps is the air entrapment at the jump toe and intense air-water mixing in the hydraulic jump roller. The air entrainment in hydraulic jumps was studied first in terms of the rate of entrained air that is a key design considerations in closed-conduit flows (KALINSKE and ROBERTSON 1943, FALVEY 1980). Some early two-phase flow measurements in hydraulic jumps were performed in India by RAJARATNAM (1962) and THANDAVESWARA (1974). An important study was that of RESCH and LEUTHEUSSER (1972) highlighting the effects of the inflow conditions. In the last fifteen years, some significant advances included CHANSON (1995,2007,2010), MOSSA and TOLVE (1998), CHANSON and BRATTBERG (2000), MURZYN et al. (2005,2007). These studies documented the vertical distributions of void fractions, bubble count rates and air-water velocities in hydraulic jumps with partially-developed inflow conditions. To date, most studies were conducted with relatively large inflow Froude numbers ($Fr_1 > 5$), but for MURZYN et al. (2005,2007), where Fr_1 is the inflow Froude number defined as:

$$Fr_1 = \frac{V_1}{\sqrt{g\,d_1}} \quad (1)$$

where V_1 and d_1 are respectively the inflow velocity and depth (Fig. 1). Recent experiments were conducted with identical inflow Froude numbers at different geometric scale, and the results indicated that data obtained with small Reynolds numbers cannot be extrapolated to large-scale hydraulic jumps without some scale effects (CHANSON and GUALTIERI 2008, MURZYN and CHANSON 2008).

It is the purpose of this paper to present a series of experimental results obtained in hydraulic jumps with relatively small Froude numbers ($2.4 < Fr_1 < 5.1$) operating at relatively large Reynolds numbers

(6.6×10^4 < Re < 1.3×10^5). First, the experimental apparatus is described in detail. Then the free-surface properties are described and the basic air-water flow properties are presented. In the later part, the longitudinal structure of the bubbly flow is discussed.

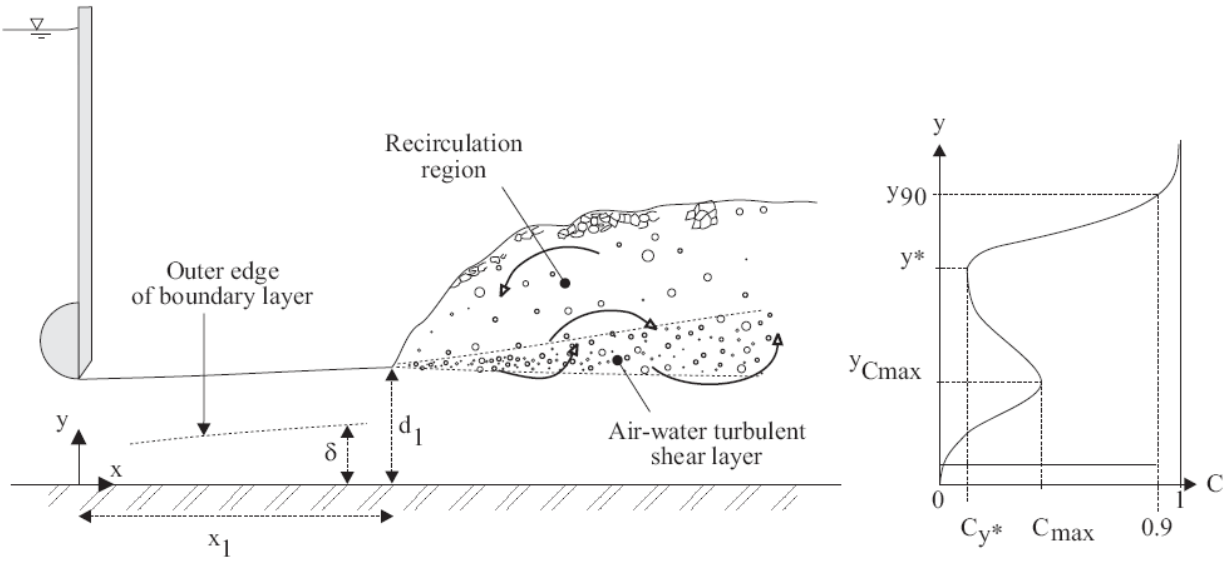

Fig. 1 - Definition sketch of a hydraulic jump with partially-developed inflow conditions

EXPERIMENTAL FACILITY AND INSTRUMENTATION

The experiments were performed at the University of Queensland. The channel was horizontal, 3.2 long and 0.5 m wide with 0.45 m high glass sidewalls, while the bed was made of 12 mm thick PVC sheets. The inflow was controlled by an upstream rounded undershoot gate. The same flume was used previously by CHANSON (2007, 2010), although new flow conditions were tested in the present study (Table 1).

The water supply was fed by a constant head tank. The water discharge was measured with a Venturi meter system located in the supply line; the discharge measurements were accurate within ±2%. The clear-water flow depths were measured using point gages with a 0.25 mm accuracy. The instantaneous free surface elevations were measured using seven ultrasonic displacement meters Microsonic™ Mic+25/IU/TC located along and above the flume centreline. The inflow conditions were controlled by a vertical undershoot gate with a semi-circular shape (∅ = 0.3 m). The upstream gate aperture was fixed during all experiments (h = 0.036 m).

Additional information was obtained with some digital cameras by CHACHEREAU and CHANSON (2010) together with the complete data sets.

Bubbly flow instrumentation

The bubbly flow properties were measured with a double-tip conductivity probe; each sensor has an inner diameter of 0.25 mm; the longitudinal distance between probe sensors was $\Delta x = 7.12$ mm. The displacement of the dual-tip probe in the vertical direction was controlled by a fine adjustment system connected to a Mitutoyo™ digimatic scale unit with a vertical accuracy of than 0.1 mm. The probe was excited by an electronic system (Ref. UQ82.518) designed with a response time of less than 10 μs. Herein each probe sensor was sampled at 20 kHz for 45 s. The analysis of the probe voltage output was based upon a single threshold technique.

The processing of the probe signal yielded a number of bubbly flow properties, including the void fraction C, the bubble count rate F defined as the number of bubbles impacting the probe sensor per second, and the bubble chord time distributions where the chord time is defined as the time spent by the bubble on the probe sensor. The air-water interfacial velocity V was calculated from a cross-correlation analysis. The turbulence level Tu characterised the fluctuations of the interfacial velocity between the probe sensors and deduced from the shapes of the cross-correlation and auto-correlation functions (CHANSON and TOOMBES 2002, CHANSON 2002). The analysis of the probe signal time series provided further information on the longitudinal air-water structure of the bubbly flow.

Experimental flow conditions

For all experiments, the jump toe was located at a distance $x_1 = 1.50$ m from the upstream rounded gate and the same gate opening $h = 0.036$ m was used for the whole study. For these conditions, the inflow depth ranged from 0.044 to 0.039 m depending upon the flow rate (Table 1, column 5).

Two series of experiments were conducted (Table 1). The first series focused on the free-surface properties of hydraulic jumps. The experiments were performed with inflow Froude numbers between 2.0 and 4.8 corresponding to Reynolds numbers between 8.8×10^4 and 1.3×10^5 In the second series of experiments, some detailed air-water flow measurements at the sub-millimetric scale were conducted

using the double-tip phase-detection probe. The flow conditions corresponded to Froude numbers between 3.1 and 5.1, considered as relatively small, and Reynolds numbers between 8.9×10^4 and 1.3×10^5, although the focus of the study was on the hydraulics jumps with relatively small Froude numbers and large Reynolds numbers ($Fr_1 < 5.1$, $Re > 6.6\times10^4$).

Table 1 - Experimental measurements in hydraulic jumps with relatively small inflow Froude numbers

Ref. (1)	Q (m^3/s) (2)	B (m) (3)	x_1 (m) (4)	d_1 (m) (5)	Fr_1 (6)	Re (7)	Remarks (8)
MURZYN et al. (2005)	0.027 to 0.014	0.30	--	0.059 to 0.021	2.0 to 4.8	8.8×10^4 to 4.6×10^4	
Present study	0.033 to 0.063	0.50	1.50	0.044 to 0.039	2.4 to 5.1	6.6×10^4 to 1.3×10^5	Free-surface measurements.
	0.045 to 0.063	0.50	1.50	0.044 to 0.0395	3.1 to 5.1	8.9×10^4 to 1.3×10^5	Air-water measurements.

Inflow conditions

In the upstream supercritical flow, the vertical distributions of velocity and pressure were measured with the Prandtl-Pitot tube. The Prandtl-Pitot tube measurements showed that the pressure distributions were hydrostatic, while the supercritical flow consisted of a developing boundary layer and an ideal fluid flow region above. That is, the hydraulic jump inflow conditions were partially-developed for all investigated flow conditions. The relative boundary layer thickness at the jump toe δ/d_o ranged from 0.12 to 0.39 when the inflow Froude number ranged from 3.1 to 5.1.

BASIC FLOW PATTERNS

For inflow Froude numbers less than 2.3, some free-surface undulations were observed: that is, the hydraulic jump was an undular hydraulic jump. For $Fr_1 > 2.4$, the hydraulic jump was characterised by a marked roller and some air bubble entrainment (Fig. 2). Downstream of the jump toe, the free surface of the hydraulic jump was strongly turbulent. Some large vertical fluctuations, foamy air-water structures and water projections were observed.

The high-shutter speed photographs and movies showed the large instantaneous air-water structures projected high above the roller surface. The short-lived structures exhibited a wide range of shapes. Figure 2 shows a series of high-shutter speed photographs aimed to illustrate the variety of short-lived air-water structures projected above the hydraulic jump. Figure 2B presents some photographs looking downstream at the jump toe, the impingement perimeter and the associated free-surface discontinuity,

and the air-water projections above the entrapment point. While a large proportion of air-water structures were projected upwards with an initially forward motion, some were ejected with the negative direction, sometimes landing upstream of the jump toe. This was highlighted by droplet impacts on the camera lens.

(A) Side view with flow from right to left - Shutter: 1/40 s at f/3.5, ISO 400

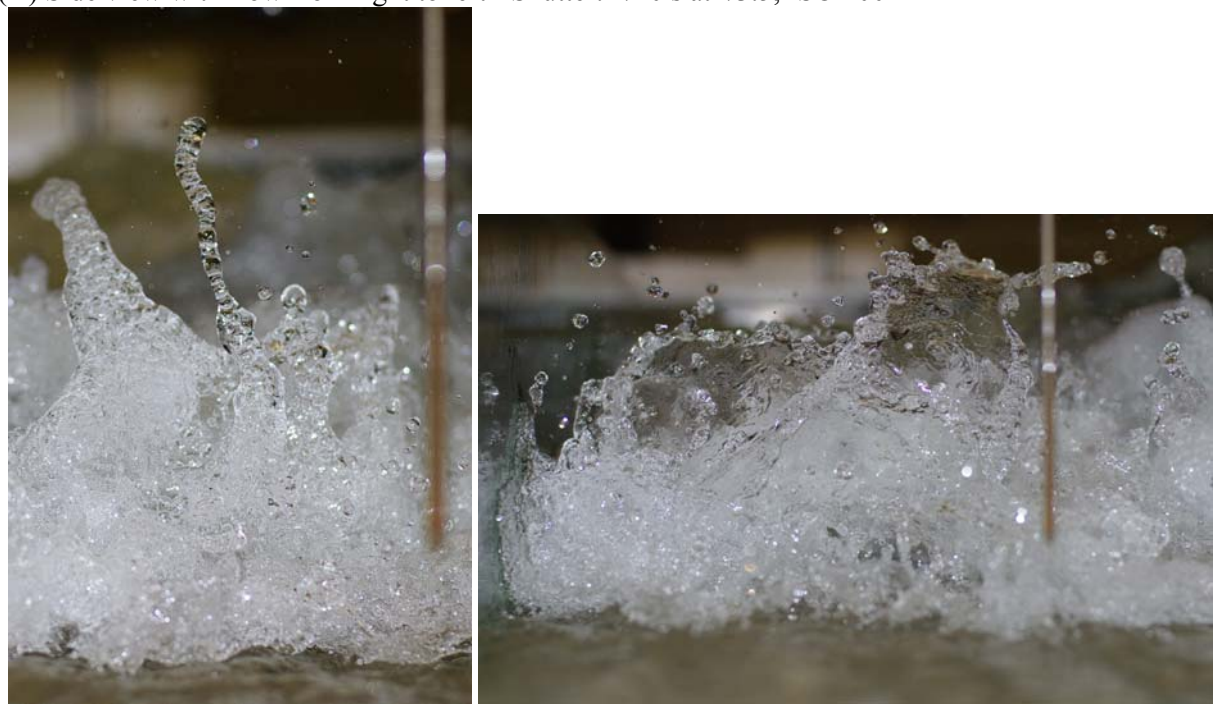

(B) Air-water projections in hydraulic jumps, looking downstream at the impingement point and free-

surface discontinuity at the jump toe - Shutter: 1/180 s at f/2.5, ISO 100

Fig. 2 - High-shutter speed photographs of air bubble entrainment and air-water projections in a hydraulic jump - d_1 = 0.0395 m, x_1 = 1.5 m, Fr_1 = 5.1, Re =1.3×10^5

FREE-SURFACE PROPERTIES

The free surface profiles were recorded for ten experiments with inflow Froude numbers ranging from 2.4 to 5.1 (Table 1). The instrumentation consisted in seven acoustic displacement meters located along and above the channel centreline, and sampled at 50 Hz for 10 minutes. Figure 3 presents some typical mean free surface profiles and standard deviations of the free-surface elevations, where η is the time-averaged free-surface elevation above the invert, η' is the standard deviation of the free-surface elevation, x is the longitudinal position of the sensor, d_1 is the inflow depth immediately upstream of the hydraulic jump toe, and x_1 is the longitudinal position of the jump toe (x_1 = 1.50 m).

The data showed some longitudinal profiles that were very close to the photographic observations through the glass sidewalls (e.g. Fig. 2A), and the results were consistent with earlier, classical results (BAKHMETEFF and MATZKE 1936, REHBOCK 1929, CASTRO-ORGUAZ and HAGER 2010).

The standard deviation of the water elevation η' characterised the turbulent fluctuations of the free surface. Although some small free-surface fluctuations were observed upstream of the jump toe ($x-x_1 < 0$), a marked increase in free surface fluctuation was observed immediately downstream of the jump toe ($x-x_1 > 0$) for all Froude numbers (Fig. 3 Right). The free-surface fluctuations reached a maximum value η'_{max}, and this maximum value η'_{max} increased with increasing Froude numbers (Fig. 3 Right). The large standard deviations in free-surface elevations were linked with a large number of air-water projections above the roller and jump toe illustrated in Figure 2B. Further downstream, the free-surface fluctuations η' decreased with increasing distance from the jump toe. The results were consistent with the earlier studies of MOUAZE et al. (2005) and MURZYN and CHANSON (2009).

The peak of turbulent fluctuations was observed in the first half of the roller as previously observed by MOUAZE et al. (2005) and MURZYN and CHANSON (2009). In Figure 3, the standard deviation of the free-surface elevation was nearly 0.3 and 0.7 times the inflow depth (0.3 d_1 and 0.7d_1) for Fr_1 = 2.8 and 5.1 respectively. Thus the free surface became more turbulent with increasing Froude number. Note

that, with the present experimental setup, an increasing Froude number was associated with an increasing Reynolds number.

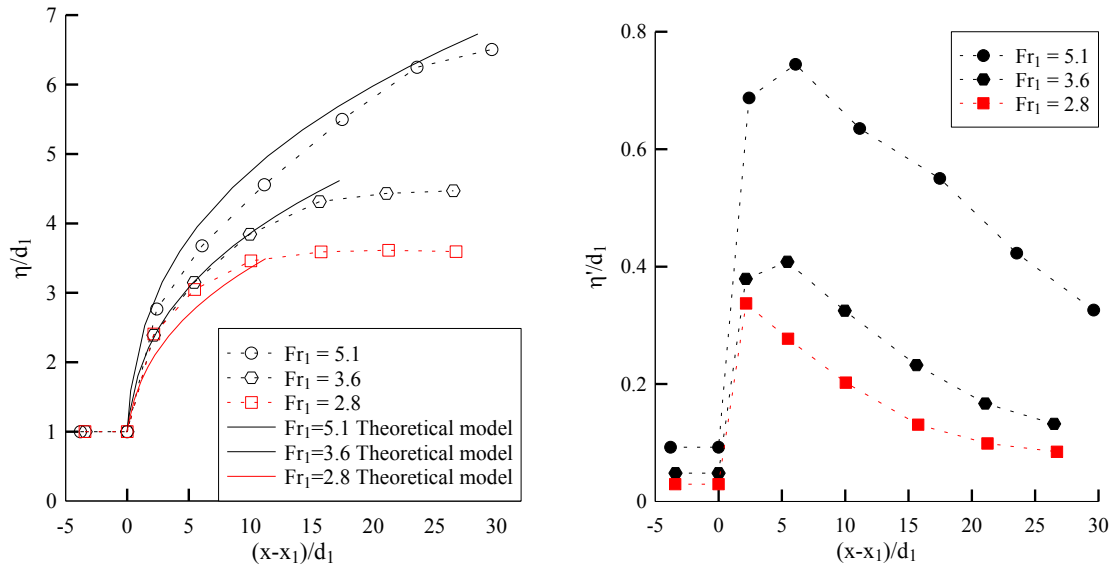

Figure 3 - Longitudinal distributions of dimensionless time-averaged free surface profile η/d_1 (Left) and standard deviation of the free surface elevations η'/d_1 (Right) - Comparison with the roller surface model of CASTRO-ORGUAZ and HAGER (2010)

A frequency analysis of the acoustic displacement meter signal outputs was performed. The results showed a dominant, characteristic frequency for all flow conditions and most longitudinal locations. For the experimental investigations (Table 1), the dominant frequencies were between 1.6 and 4 Hz, with a large majority between 1.8 and 3 Hz, and the results showed relatively little effect of the longitudinal distance $(x-x_1)/d_1$. Figure 4 summarises the characteristic free-surface fluctuation frequency in the hydraulic jump roller as a function of the inflow Froude number. The data are shown with the range of data scatter and compared with the data of MURZYN and CHANSON (2009) obtained with the same type of instrumentation, same sampling rate and duration. Despite some scatter, all the data decrease in dimensionless free-surface frequency with increasing Froude number, and they were best correlated by:

$$\frac{F_{fs}\ d_1}{V_1} = 0.143 \exp(-0.27\ Fr_1) \qquad 2.4 < Fr_1 < 6.5 \quad (1)$$

with a normalised correlation coefficient of 0.62. Equation (2) is compared with the data in Figure 2.

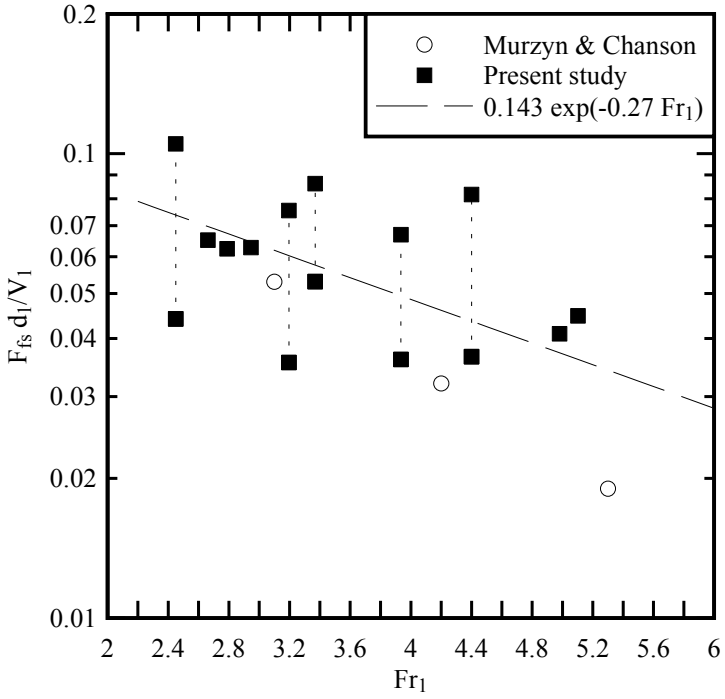

Fig. 4 - Dimensionless characteristic free-surface fluctuation frequency $F_{fs}d_1/V_1$ as a function of the inflow Froude number - Comparison with the experimental data of MURZYN and CHANSON (2009)

BUBBLY FLOW PROPERTIES

Void fraction and bubble count rate distributions

In the hydraulic jump roller, two distinct air-water flow regions were identified: the lower region dominated by the developing turbulent shear layer; and the upper part consisting in the free surface region characterised by large void fraction, splashes and recirculation areas. Figure 5A presents some typical void fraction distributions in the roller of hydraulic jumps with partially-developed inflow conditions. The void fraction C reached a local maximum C_{max} in the air-water shear layer at an elevation y_{Cmax}, and the elevation y* marked the vertical elevation above which the void fraction increased monotically to unity (Fig. 1, Right). In the developing shear layer, the void fraction data were compared with an analytical solution of the advective diffusion equation for air bubble in a uniform flow (CHANSON 1995,2010):

$$C = C_{max} \exp\left(- \frac{\left(\frac{y - y_{C\,max}}{d_1} \right)^2}{4D^{\#}\left(\frac{x - x_1}{d_1} \right)} \right) \quad (3)$$

where $D^{\#}$ is the dimensionless turbulent diffusivity: $D^{\#} = D_t/(V_1 d_1)$, D_t is the turbulent diffusivity assumed constant at a given longitudinal position, and d_1 and V_1 are respectively the inflow depth and velocity. Figure 5A presents some typical void fraction profiles at different longitudinal locations for a given Froude number, and the data are compared with Equation (3). Although the advective diffusion equation is based upon the crude assumptions of constant diffusivity D# and product $C_{max}\sqrt{(x - x_1)/d_1}$, the physical data (MURZYN et al. 2005, Present study) showed some agreement with Equation (3).

In the developing shear layer, the maximum void fraction C_{max} decreased with increasing distance from the impingement point (x-x_1) (Fig. 6A). Figure 6A presents the evolution of C_{max} with the dimensionless streamwise position. The full data set is reported in Appendix I. The data showed some effect of the inflow Froude number, and they are compared with earlier experimental data by CHANSON (2007,2010) for a Froude number of 5.1. A good agreement was observed between the different sets of data. The experimental data exhibited a behaviour that was correlated by:

$$C_{max} = \frac{0.056 \times Fr_1 + 0.0106}{\sqrt{\frac{x - x_1}{d_1}}} \qquad 3.1 < Fr_1 < 5.1 \quad (4)$$

Equation (4) is shown in Figure 6A for a Froude number. The depth-averaged void fraction C_{mean} is another parameter describing the rate of air entrainment in the hydraulic jump. The depth-averaged void fraction C_{mean} is defined as:

$$C_{mean} = \frac{1}{y_{90}} \int_0^{y_{90}} C \, dy \quad (5)$$

where y_{90} is the vertical elevation corresponding to a void fraction of 90% (Fig. 1, Right). For $y > y_{90}$, the liquid fraction corresponded primarily to splashing. C_{mean} ranged from 0.30 down to 0.03. The full data set is reported in Appendix I. The experimental results showed some decrease in depth-averaged void fraction with increasing distance from the jump toe, as buoyancy effects induced some bubble migration towards the free surface associated with some de-aeration of the flow.

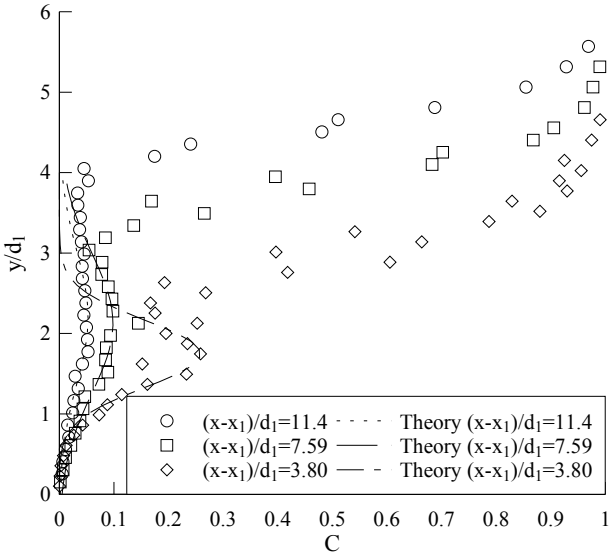

(A) Void fraction distributions

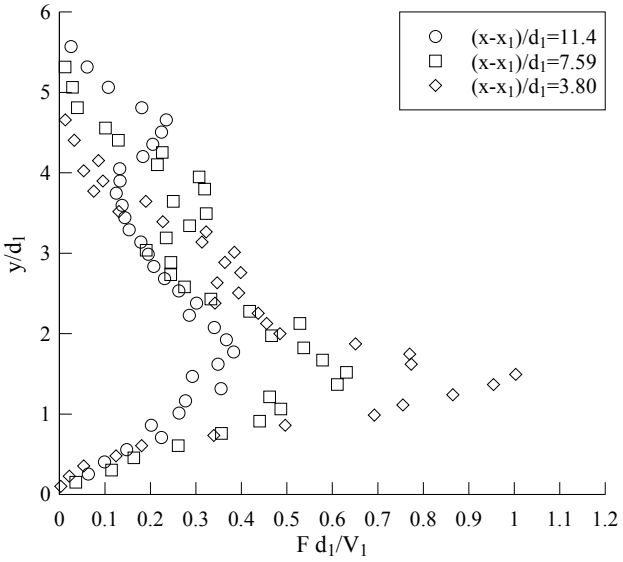

(B) Bubble count rate distributions

Figure 5 - Dimensionless distributions of void fraction and bubble count rate in a hydraulic jump - d_1 = 0.0395 m, Fr_1 = 4.4, Re = 1.1×10^5

The dimensionless turbulent diffusivity $D^{\#}$ (Eq. (3)) was estimated at all longitudinal locations for all flow conditions. The values of the dimensionless coefficient $D^{\#}$ ranged between 0.017 and 0.060, corresponding to D_t between 0.0028 and 0.0059 m^2/s (Table 2). Despite some scatter, the dimensionless turbulent diffusivity data $D^{\#}$ were comparable with the results of CHANSON and BRATTBERG (2000)

and CHANSON (2010) for comparable Froude numbers. The results were basically independent of the longitudinal distance from the jump toe (Table 2). Similarly the product $C_{max}\sqrt{(x-x_1)/d_1}$ is reported in Table 2 indicating little variation with longitudinal distance. The findings differed from the experimental data trend obtained in hydraulic jumps with large Froude numbers (CHANSON 2010).

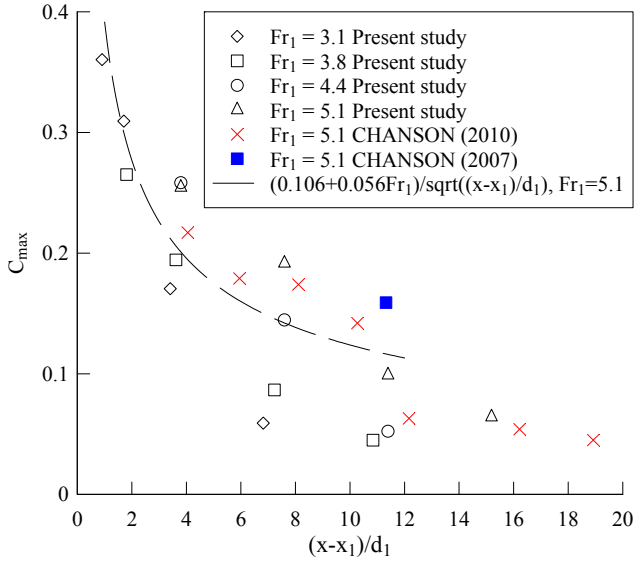

(A) Maximum void fraction C_{max} in the air-water shear layer

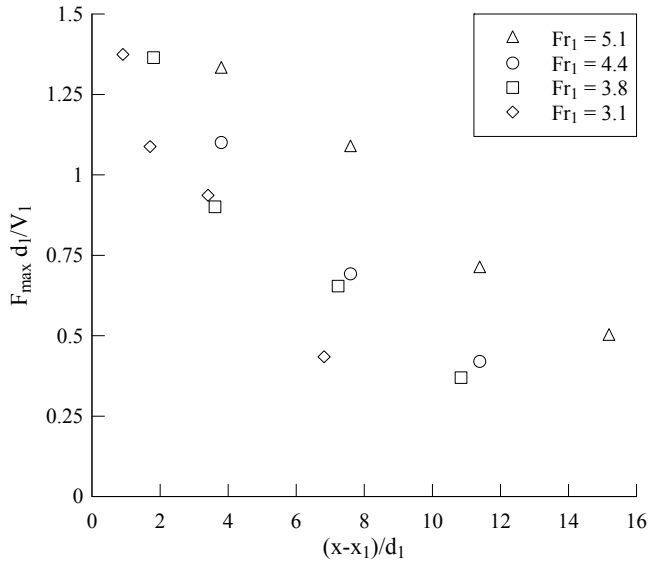

(B) Maximum bubble count rate $F_{max}d_1/V_1$ in the air-water shear layer

Figure 6 - Dimensionless longitudinal distribution of maximum void fraction, depth-averaged void fraction and maximum bubble count rate in the air-water shear layer - Comparison between experimental data and Equation (4) for $Fr_1 = 5.1$

CHACHERAU, Y., and CHANSON, H. (2011). "Bubbly Flow Measurements in Hydraulic Jumps with Small Inflow Froude Numbers." *International Journal of Multiphase Flow*, Vol. 37, No. 6, pp. 555-564 (DOI: 10.1016/j.ijmultiphaseflow.2011.03.012) (ISSN 0301-9322).

Table 2 - Turbulent diffusivity coefficient and maximum void fraction in the developing shear layer (Present study)

x_1 (m)	d_1 (m)	Fr_1	Re	$(x-x_1)/d_1$	$D^{\#}$	D_t (m^2/s)	$C_{max}\sqrt{\frac{x-x_1}{d_1}}$
1.50	0.044	3.1	8.9×10^4	0.91	0.022	0.0020	0.344
				1.70	0.017	0.0015	0.403
				3.41	0.030	0.0027	0.315
				6.82	0.030	0.0027	0.154
1.50	0.0405	3.8	9.8×10^4	1.81	0.040	0.0039	0.357
				3.81	0.060	0.0059	0.379
				7.23	0.030	0.0029	0.233
				10.8	0.030	0.0029	0.148
1.50	0.0395	4.4	1.1×10^5	3.80	0.023	0.0025	0.504
				7.59	0.050	0.0055	0.398
				11.4	0.030	0.0033	0.177
1.50	0.0395	5.1	1.3×10^5	3.80	0.022	0.0028	0.498
				7.59	0.040	0.0050	0.528
				11.4	0.050	0.0063	0.334
				15.2	0.035	0.0044	0.250

Note: D_t was derived from the best fit between the void fraction data and Equation (3).

The bubble count rate F was defined as the number of air bubbles detected by the conductivity probe leading tip per unit time at a given location. Figure 5B presents some typical vertical distributions of dimensionless bubble count rates $F\ d_1/V_1$. The data presented some profiles that were comparable to the earlier results of CHANSON and BRATTBERG (2000), MURZYN et al. (2005), CHANSON (2007), and MURZYN and CHANSON (2009). They highlighted a maximum bubble count rate F_{max} in the air-water shear layer. The peak in bubble count rate F_{max} was likely linked with the large turbulent shear stresses that break up the entrained bubbles into finer particles. The small air entities entrained by the high velocities in the air-water shear flow resulted in an important number of bubbles impacting the conductivity probe tips. Figure 6B presents the maximum bubble count rate F_{max} as a function of the dimensionless distance to the toe for all Froude numbers. The full data set is reported in Appendix I. The experimental results showed that the maximum count rate F_{max} decreased with increasing distance from the jump toe for a given inflow Froude number; it was seen also to increase with increasing Froude number at a given location.

Velocity and turbulent intensity distributions

The air-water interfacial velocity was measured with the dual-tip conductivity probe. The cross-correlation function between the signals from both tips provided the average travel time between the probe sensors. However, in the flow regions where the sign of the velocity changed rapidly during the sampling period (45 s), no meaningful travel time could be derived from the cross-correlation analyses. This was typical in the upper shear layer. In the recirculation region, some negative velocities were recorded, although the two tips of the conductivity probe were behind the support of the probe and the result might be affected by the support wake.

Figure 7 presents some typical dimensionless distributions of interfacial velocities V/V_1 in the roller, where V_1 is the depth-averaged inflow velocity. In each figure, the zero lines for the velocity origin were shown in dashed. The experimental results highlighted some key features for all inflow Froude numbers. Namely, the high-velocity jet for $y/d_1 < 1$, the shear zone with a high-velocity gradient $\partial V/\partial y$, and the recirculation region above where $V < 0$.

The dimensionless distributions of interfacial velocities followed closely:

$$\frac{V}{V_{max}} = \left(\frac{y}{Y_{V\,max}}\right)^{\frac{1}{N}} \qquad \text{for } \frac{y}{yY_{V\,max}} < 1 \quad (6a)$$

$$\frac{V - V_{recirc}}{V_{max} - V_{recirc}} = \exp\left(-\frac{1}{2}\left[1.765\left(\frac{y - Y_{V\,max}}{y_{0.5}}\right)\right]^2\right) \qquad \text{for } 1 < \frac{y}{Y_{V\,max}} < 3 \text{ to } 4 \quad (6b)$$

where V_{max} is the maximum velocity in the shear layer observed at $y = y_{Vmax}$, V_{recirc} is the recirculation velocity measured in the upper free-surface region, $y_{0.5}$ is the vertical elevation where $V = V_{max}/2$ and N is a constant ($N \approx 6$). Despite some data scatter, the data trend followed closely Equation (6) (not shown in Fig. 7 for clarity) and the characteristic velocity distribution parameters are reported in Appendix I.

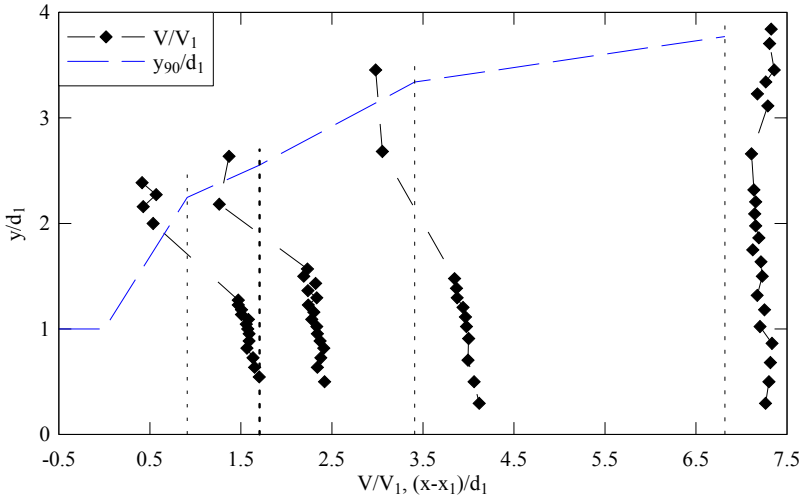

(A) $Fr_1 = 3.1$, $Re = 8.9 \times 10^4$, $d_1 = 0.044$ m, $x_1 = 1.50$ m

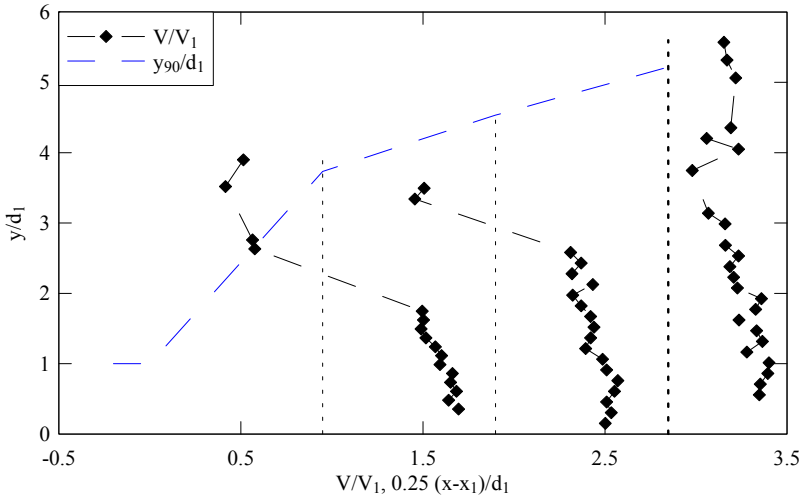

(B) $Fr_1 = 4.4$, $Re = 1.1 \times 10^5$, $d_1 = 0.0395$ m, $x_1 = 1.50$ m

Figure 7 - Dimensionless velocity distributions in the hydraulics jump roller

The turbulence level characterised the fluctuations of the longitudinal velocity component. The turbulence intensity was derived from a cross correlation analysis between the two probe sensor signals. The method was based on the relative width of the auto- and cross-correlation functions (CHANSON and TOOMBES 2002). Figure 8 presents some typical distributions of the turbulence intensity in the investigated hydraulic jumps. The turbulence levels were seen to decrease with increasing distance from the jump toe for a given Froude number. Within a cross section, Tu increased with increasing distance from the bed.

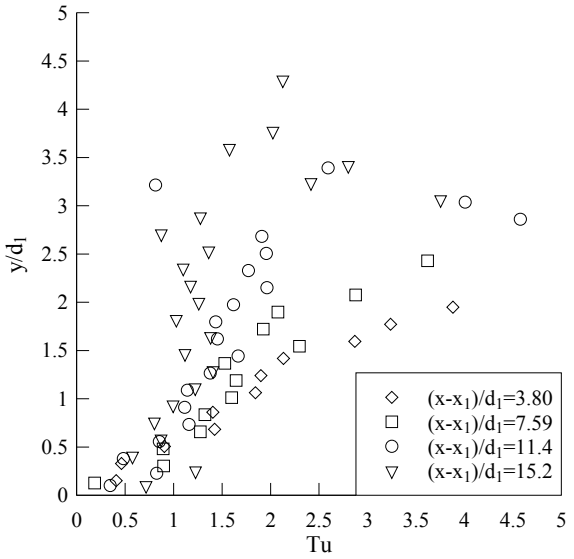

Figure 8 - Dimensionless distributions of streamwise turbulence intensity Tu in hydraulic jump rollers - $Fr_1 = 5.1$, $Re = 1.3 \times 10^5$, $d_1 = 0.0395$ m, $x_1 = 1.50$ m

BUBBLE CHORD PROPERTIES

Bubble chord time distributions

The probability distribution functions of bubble chord times were investigated. The bubble chord time was defined as the time spent by the bubble on the probe tip. The small bubble chord times corresponded to small bubbles passing rapidly on the probe tips, while large chord times implied large air packets flowing slowly past the probe sensor. Figure 9 presents the probability distribution function of the bubble chord times at the elevation y_{Fmax}, where the bubble count rate was maximum ($F = F_{max}$). The data are presented as a series of histograms, and each histogram column represents the probability of bubble chord time in a 0.5 ms chord time interval. For example, the probability of bubble chord time between 1 and 1.5 ms is represented by the column labelled 1 ms. Bubble chord times larger than 10 ms are regrouped in the last column. The experimental data showed a broad spectrum of chord times at the investigated locations. The bubble chord times measured ranged from less than 0.5 ms to more than 10 ms. The chord times smaller than 2 ms were clearly predominant in every case with the largest probability between 0.5 and 1 ms.

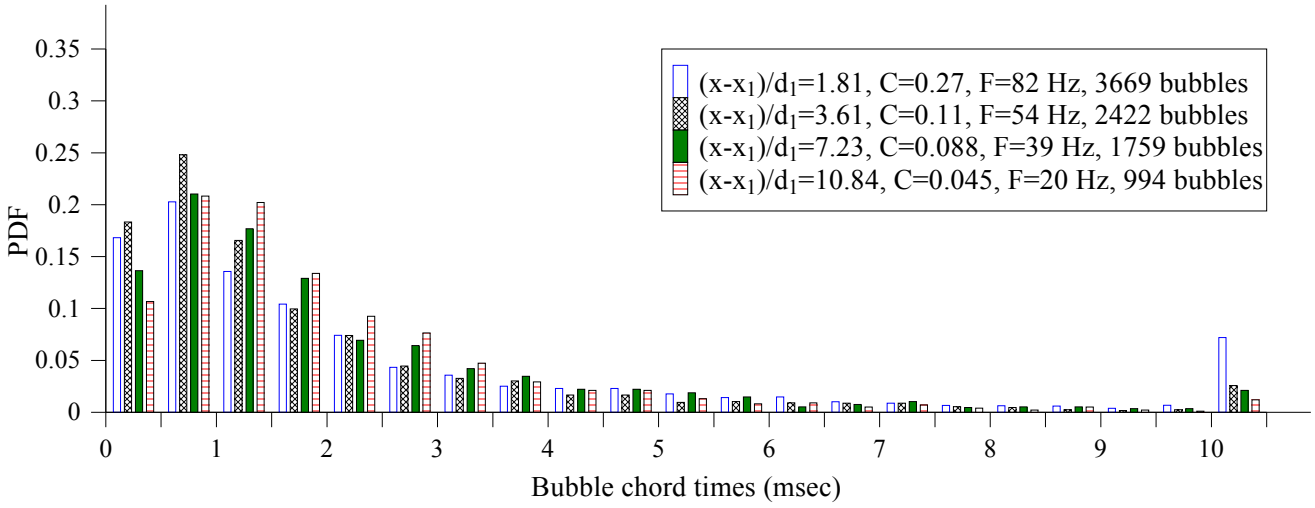

(A) Fr_1 = 3.8

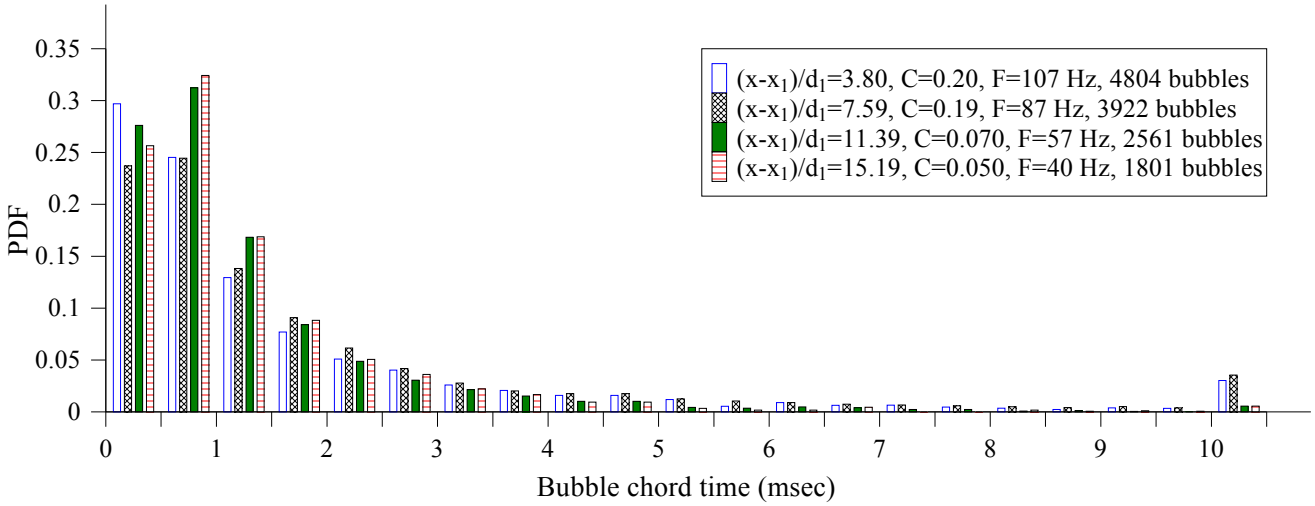

(B) Fr_1 = 5.1

Figure 9 - Bubble chord time distributions at the characteristic elevation y_{Fmax} where $F = F_{max}$ in the air-water shear layer of hydraulic jumps

Bubble clustering

The entrained bubbles interact with the turbulence structures, yielding to some turbulent dissipation and the formation of bubble clusters (CHANSON 2007). The study of bubble clustering is relevant to infer whether the formation frequency responds to some particular frequencies of the flow. In hydraulic jumps, the clustering index may provide a measure of the vorticity production rate, of the level of bubble-turbulence interactions and of the associated energy dissipation. Altogether both macro- and micro-scopic air-water flow properties are required to characterise completely the hydraulic jump flow.

The present experimental results demonstrated a broad spectrum of bubble chord times extending over several orders of magnitude and the distributions of chord times were skewed with a preponderance of small bubbles relative to the mean (Fig. 9). Some advanced signal processing provided further information on the longitudinal structure of the air-water flow including bubble clustering. When two bubbles are closer than a particular time/length scale, they can be considered a group of bubbles: i.e., a cluster. The characteristic water time/length scale may be related to the water chord statistics or to the near-wake of the preceding particle. Herein the latter approach was applied following CHANSON et al. (2006) and CHANSON (2010). Two bubbles were considered parts of a cluster when the water chord time between two consecutive bubbles was less than the lead bubble chord time. Simply, when a bubble trailed the previous bubble by a short time/length, it was in the near-wake of and could be influenced by the leading particle. Note that the criterion is based upon a comparison between the local, instantaneous characteristic time scales of the air-water flow. It did not rely upon the velocity measurement technique, but it implies that the streamwise velocity is positive. Further the criterion is independent of the local air-water flow properties.

Figure 10 presents some typical characteristic properties of the bubble clusters in the developing shear layer. All the data were recorded at the characteristic location ($y = y_{Fmax}$) where the bubble count rate was maximum ($F = F_{max}$). Figure 10 includes the longitudinal distributions of number of clusters per second, the percentage of bubbles in clusters, the average number of bubbles per cluster, the probability distribution function of the number of bubbles per cluster (for $Fr_1 = 3.1$), and the ratio of lead bubble chord to average cluster bubble chord.

The experimental results showed systematically a number of trends. The number of clusters per second was substantial in the air-water shear layer, reaching up to 22 clusters per second for $Fr_1 = 5.1$. Further the number of clusters decreased rapidly with increasing longitudinal distance (Fig.10A). The present data showed an exponential decay in the number of clusters:

$$\frac{N_c \, d_1}{V_1} \propto \exp\left(-\frac{x - x_1}{d_1}\right) \quad (7)$$

where N_c is the number of clusters per second.

The experimental results highlighted that a large proportion of bubbles were parts of a cluster structure in the air-water shear zone. That is, up to half of all bubbles at the beginning of the shear layer ((x-

$x_1)/d_1 < 5$), and the percentage of bubbles in clusters decreased with increasing longitudinal distance (Fig. 10B). The present findings differed from the results of CHANSON (2010), with hydraulic jumps at large Froude numbers, who found up to one third of bubbles in clusters. It is believed that the key difference was the differences in Froude numbers as well as the larger Reynolds number range investigated herein ($9\times10^4 < Re < 1.3\times10^5$).

On average, the number of bubbles per cluster ranged from 2.7 down to 2.3 and decreased with increasing distance from the jump toe (Fig. 10C). The longitudinal pattern is illustrated in Figure 10D showing the probability distribution function of the number of bubbles per clusters at four longitudinal locations for one experiment ($Fr_1 = 3.1$). In a cluster, the lead bubble was followed by a group of bubbles. Figure 10E presents the ratio of the lead bubble chord to average cluster bubble chord. The data showed that the lead bubble chord was larger on average that the typical cluster bubble chord; the ratio of lead bubble chord to mean cluster bubble chord ranged from 1.4 down to 1.15, decreasing with increasing distance from the jump toe (Fig. 10E).

It is important to stress however that the present data analysis was focused on the longitudinal air-water structure and did not consider any bubble travelling side-by-side.

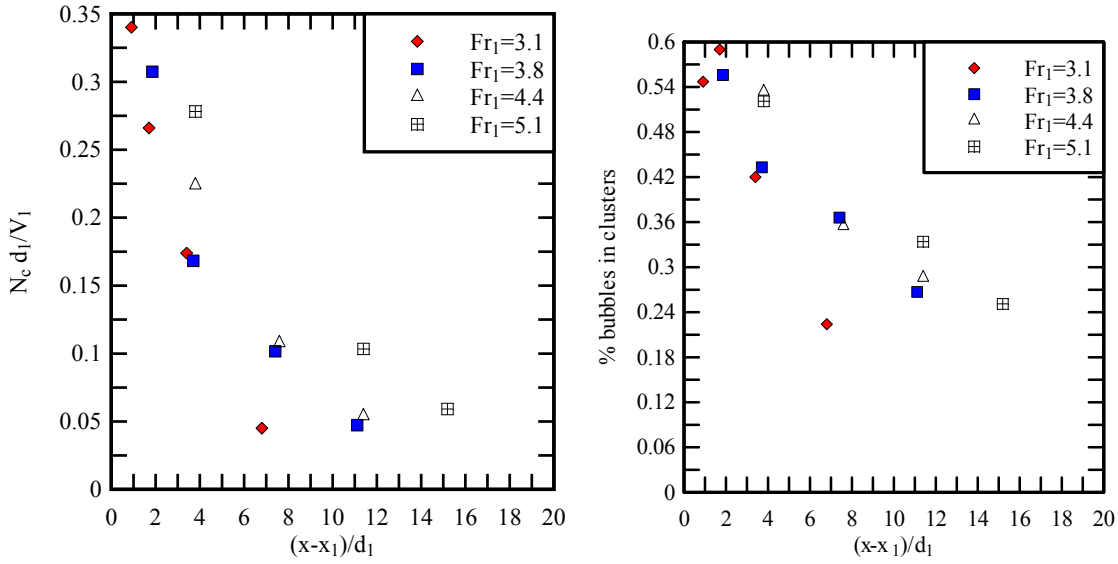

(A, Left) Dimensionless number of cluster per second $N_c d_1/V_1$

(B, Right) Percentage of bubbles in clusters

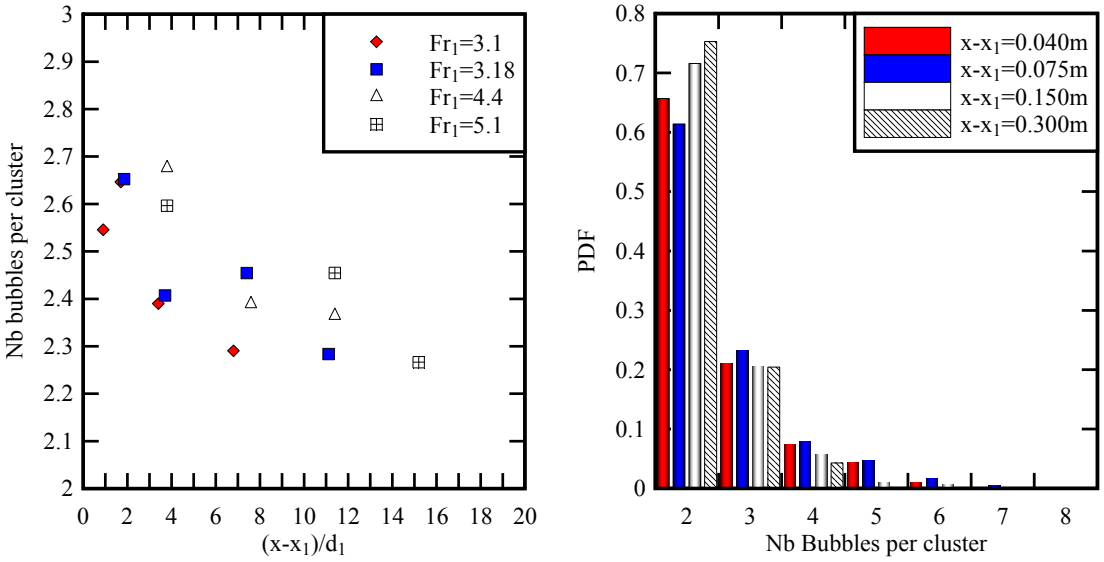

(C, Left) Number of bubbles per cluster

(D, Right) Probability distribution functions of the number of bubbles per cluster for $Fr_1 = 3.1$

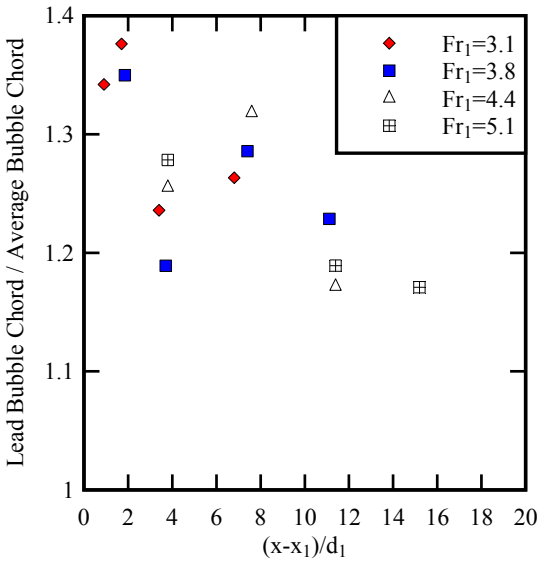

(E) Ratio of lead bubble chord to average cluster bubble chord

Figure 10 - Characteristic properties of bubble clusters in the air-water shear layer at the locations where $F = F_{max}$ ($y = y_{Fmax}$)

A comparative analysis was further performed on the chord times of cluster bubbles and the whole bubble population. The distributions of bubble chord times showed only some small differences between the bubbles in cluster structures and the whole bubble population. There was no obvious preferential bubble chord times in the clusters. The findings contradict the results of CHANSON (2007)

based upon an inter-particle arrival time analysis. It is believed that some assumptions underlying the inter-particle arrival time analysis were incorrect in the developing shear layer of hydraulic jumps (EDWARDS and MARX 1995). The method assumed an ideal dispersed flow driven by a superposition of Poisson processes assuming non-interacting particles. In the air-water shear layer, the bubbles were subjected to a wide range of interactions including bubble trapping in the large coherent structure, breakup by turbulent shear, bubble collisions and bubble coalescence.

CONCLUSION

A hydraulic jump is a complex turbulent phenomenon that remains incompletely understood. The turbulent flow regions include a developing shear layer, the roller and the air-water interface. In the present study, both the free surface fluctuations and air-water properties were investigated physically in hydraulic jumps with relatively small Froude numbers ($2.4 < Fr_1 < 5.1$) and relatively large Reynolds numbers ($6.6 \times 10^4 < Re < 1.3 \times 10^5$). The dynamic free surface measurements were performed with acoustic displacement meters to record non-intrusively the mean and turbulent surface profiles, and their characteristic frequencies. The two-phase flow measurements were conducted with a dual-tip conductivity probe.

The free surface fluctuations were investigated for upstream Froude numbers between 2.4 and 5.1. Both the mean and turbulent free surface profiles were recorded. The turbulent fluctuation profiles exhibited a peak of maximum intensity in the first half of the hydraulic jump roller, and its amplitude increased monotically with increasing Froude number. The free surface fluctuations exhibited some characteristic frequencies typically below 3 Hz. The data sets demonstrated to the intense free-surface fluctuations of the roller and the findings were consistent with earlier studies.

In the air-water roller region, the data highlighted two characteristic regions: the air-water shear layer in the lower part of the jump and an upper free-surface region above. The air-water shear zone was characterised by local maxima in terms of void fraction and bubble count rate, denoted C_{max} and F_{max} respectively. The mean and turbulent velocity data showed the intense turbulence in the shear zone. The probability distribution functions (PDF) of bubble chord time highlighted a broad spectrum of bubble chords, with a majority of bubble chord times between 0.5 and 2 ms. An analysis of the longitudinal air-

water structure indicated a significant proportion of bubbles travelling within a cluster structure. The findings implied some strong interactions between the entrained air bubbles and turbulence structures, particularly next to the impingement point, although the study was limited to four inflow Froude numbers ($3.1 < Fr_1 < 5.1$).

The present results complemented the earlier study of MURZYN et al. (2005) conducted with relatively low Froude numbers and the study of CHANSON (2010) performed with large Froude numbers.

ACKNOWLEDGMENTS

The authors thank Dr Frédéric MURZYN (ESTACA Laval, France) for his valuable comments. They thank further Graham ILLIDGE, Ahmed IBRAHIM, and Clive BOOTH (The University of Queensland) for their technical assistance. The writers thank Stefan FELDER (The University of Queensland) for providing his homemade programs which facilitated greatly the analysis of the air-water flow data. The financial support of the Australian Research Council (Grant DP0878922) is acknowledged.

REFERENCES

BAKHMETEFF, B.A., and MATZKE, A.E. (1936). "The Hydraulic Jump in Terms of Dynamic Similarity." *Transactions,* ASCE, Vol. 101, pp. 630-647. Discussion : Vol. 101, pp. 648-680.

CASTRO-ORGUAZ, O., and HAGER, W. (2010). "Classical Hydraulic Jump: Basic Flow Features." *Jl of Hyd. Res.*, IAHR, Vol. 47, No. 6, pp. 744-754.

CHACHEREAU, Y., and CHANSON, H., (2010). "Free-Surface Turbulent Fluctuations and Air-Water Flow Measurements in Hydraulics Jumps with Small Inflow Froude Numbers." *Hydraulic Model Report No. CH78/10*, School of Civil Engineering, The University of Queensland, Brisbane, Australia, 133 pages.

CHANSON, H. (1995). "Air Entrainment in Two-Dimensional Turbulent Shear Flows with Partially Developed Inflow Conditions." *International Journal of Multiphase Flow*, Vol. 21, No. 6, pp. 1107-1121.

CHACHERAU, Y., and CHANSON, H. (2011). "Bubbly Flow Measurements in Hydraulic Jumps with Small Inflow Froude Numbers." *International Journal of Multiphase Flow*, Vol. 37, No. 6, pp. 555-564 (DOI: 10.1016/j.ijmultiphaseflow.2011.03.012) (ISSN 0301-9322).

CHANSON, H. (2002). "Air-Water Flow Measurements with Intrusive Phase-Detection Probes. Can we Improve their Interpretation?" *Journal of Hydraulic Engineering*, Trans. ASCE, Vol. 128, No. 3, pp. 252-255

CHANSON, H. (2007). "Bubbly Flow Structure in Hydraulic Jump." *European Journal of Mechanics B/Fluids*, Vol. 26, No. 3, pp.367-384 (DOI: 10.1016/j.euromechflu.2006.08.001).

CHANSON, H. (2009). "Current Knowledge In Hydraulic Jumps And Related Phenomena. A Survey of Experimental Results." *European Journal of Mechanics B/Fluids*, Vol. 28, No. 2, pp. 191-210 (DOI: 10.1016/j.euromechflu.2008.06.004).

CHANSON, H. (2010). "Convective Transport of Air Bubbles in Strong Hydraulic Jumps." *International Journal of Multiphase Flow*, Vol. 36, No. 10, pp. 798-814 (DOI: 10.1016/j.ijmultiphaseflow.2010.05.006)

CHANSON, H., AOKI, S., and HOQUE, A. (2006). "Bubble Entrainment and Dispersion in Plunging Jet Flows: Freshwater versus Seawater." *Journal of Coastal Research*, Vol. 22, No. 3, May, pp. 664-677 (DOI: 10.2112/03-0112.1).

CHANSON, H., and BRATTBERG, T. (2000). "Experimental Study of the Air-Water Shear Flow in a Hydraulic Jump." *International Journal of Multiphase Flow*, Vol. 26, No. 4, pp. 583-607.

CHANSON, H., and GUALTIERI, C. (2008). "Similitude and Scale Effects of Air Entrainment in Hydraulic Jumps." *Journal of Hydraulic Research*, IAHR, Vol. 46, No. 1, pp. 35-44.

CHANSON, H., and TOOMBES, L. (2002). "Air-Water Flows down Stepped chutes: Turbulence and Flow Structure Observations." *International Journal of Multiphase Flow*, Vol. 28, No. 11, pp. 1737-1761.

EDWARDS, C.F., and MARX, K.D. (1995). "Multipoint Statistical Structure of the Ideal Spray, Part I: Fundamental Concepts and the Realization Density." *Atomization & Sprays*, Vol. 5, pp. 435-455.

FALVEY, H.T. (1980). "Air-Water Flow in Hydraulic Structures." *USBR Engrg. Monograph*, No. 41, Denver, Colorado, USA.

HAGER, W.H. (1992). "Energy Dissipators and Hydraulic Jump." *Kluwer Academic Publ.*, Water Science and Technology Library, Vol. 8, Dordrecht, The Netherlands, 288 pages.

KALINSKE, A.A., and ROBERTSON, J.M. (1943). "Closed Conduit Flow." *Transactions*, ASCE, Vol.

108, pp. 1435-1447.

MOSSA, M., and TOLVE, U. (1998). "Flow Visualization in Bubbly Two-Phase Hydraulic Jump." *Jl Fluids Eng.*, ASME, Vol. 120, March, pp. 160-165.

MOUAZE, D., MURZYN, F., and CHAPLIN, J.R. (2005). "Free Surface Length Scale Estimation in Hydraulic Jumps." *Journal of Fluids Engineering*, Trans. ASME, Vol. 127, pp. 1191-1193.

MURZYN, F., and CHANSON, H. (2008). "Experimental Assessment of Scale Effects Affecting Two-Phase Flow Properties in Hydraulic Jumps." *Experiments in Fluids*, Vol. 45, No. 3, pp. 513-521 (DOI: 10.1007/s00348-008-0494-4).

MURZYN, F., and CHANSON, H. (2009). "Free-Surface Fluctuations in Hydraulic Jumps: Experimental Observations." *Experimental Thermal and Fluid Science*, Vol. 33, No. 7, pp. 1055-1064 (DOI: 10.1016/j.expthermflusci.2009.06.003).

MURZYN, F., MOUAZE, D., and CHAPLIN, J.R. (2005). "Optical Fibre Probe Measurements of Bubbly Flow in Hydraulic Jumps." *International Journal of Multiphase Flow*, Vol. 31, No. 1, pp. 141-154.

MURZYN, F., MOUAZE, D., and CHAPLIN, J.R. (2007). "Air-Water Interface Dynamic and Free Surface Features in Hydraulic Jumps." *Journal of Hydraulic Research*, IAHR, Vol. 45, No. 5, pp. 679-685.

RAJARATNAM, N. (1962). "An Experimental Study of Air Entrainment Characteristics of the Hydraulic Jump." *Journal of Instn. Eng. India*, Vol. 42, No. 7, March, pp. 247-273.

REHBOCK, T. (1929). "The River Hydraulic Laboratory of the Technical University of Karlsruhe." in *Hydraulic Laboratory Practice*, ASME, New York, USA, pp. 111-242.

RESCH, F.J., and LEUTHEUSSER, H.J. (1972). "Le Ressaut Hydraulique : mesure de Turbulence dans la Région Diphasique. " ('The Hydraulic Jump: Turbulence Measurements in the Two- Phase Flow Region.'), *La Houille Blanche*, No. 4, pp. 279-293 (in French).

THANDAVESWARA, B.S. (1974). "Self Aerated Flow Characteristics in Developing Zones and in Hydraulic Jumps." *Ph.D. thesis*, Dept. of Civil Engrg., Indian Institute of Science, Bangalore, India, 399 pages.

CHACHERAU, Y., and CHANSON, H. (2011). "Bubbly Flow Measurements in Hydraulic Jumps with Small Inflow Froude Numbers." *International Journal of Multiphase Flow*, Vol. 37, No. 6, pp. 555-564 (DOI: 10.1016/j.ijmultiphaseflow.2011.03.012) (ISSN 0301-9322).

APPENDIX I - CHARACTERISTIC AIR-WATER FLOW PROPERTIES IN HYDRAULIC JUMPS (PRESENT STUDY)

Q m^3/s	d_1 m	Fr_1	$x-x_1$ m	C_{max}	y_{Cmax} mm	y* mm	C_{y*}	F_{max} Hz	y_{Fmax} mm	C_{Fmax}	F_2 Hz	y_{F2} mm	C_{F2}	V_{max} m/s	y_{Vmax} mm	$y_{0.5}$ mm	V_{recirc} m/s	y_{90} mm	C_{mean}
0.0627	0.0395	5.10	0.15	0.255	63.0	91.0	0.189	106.76	49.0	0.203	30.16	119.0	0.541	2.64	20.0	92.7	-1.16	153.6	0.373
			0.3	0.155	82.0	131.0	0.108	87.16	61.0	0.192	27.80	138.0	0.254	2.41	16.0	107.7	-1.56	194.6	0.284
			0.45	0.099	99.0	148.0	0.060	56.91	57.0	0.070	25.64	169.0	0.395	2.19	29.0	--	none	210.9	0.221
			0.6	0.064	93.0	156.0	0.028	40.02	65.0	0.050	21.40	177.0	0.203	1.95	23.0	--	none	230.6	0.194
0.0545	0.0395	4.43	0.15	0.258	69.0	94.0	0.167	76.89	59.0	0.233	30.56	109.0	0.418	2.26	14.0	79.4	-1.62	147.5	0.300
			0.3	0.145	84.0	120.0	0.054	48.38	60.0	0.089	24.73	138.0	0.265	2.03	30.0	109.2	-1.34	179.1	0.208
			0.45	0.052	70.0	148.0	0.033	29.36	70.0	0.524	18.02	184.0	0.511	1.70	112.0	--	none	206.1	0.184
0.0490	0.0405	3.84	0.075	0.265	53.5	81.0	0.186	81.53	52.0	0.265	30.33	88.0	0.404	2.06	20.0	75.0	-1.76	112.8	0.255
			0.15	0.194	84.0	96.0	0.126	53.82	48.0	0.112	28.20	114.0	0.523	2.01	30.0	84.9	-1.41	134.1	0.223
			0.3	0.087	74.0	116.0	0.058	39.09	60.0	0.879	20.20	144.0	0.420	1.72	--	--	none	169.8	0.197
			0.45	0.045	67.0	148.0	0.335	22.09	67.0	0.045	15.47	169.0	0.233	1.48	--	--	none	195.6	0.153
0.0446	0.0441	3.08	0.04	0.360	58.0	73.0	0.305	63.33	48.0	0.241	32.67	76.0	0.414	1.96	24.0	65.6	-1.23	98.8	0.243
			0.075	0.309	54.0	84.0	0.210	50.13	54.0	0.309	29.47	90.0	0.370	1.75	36.0	76.3	-1.09	112.4	0.288
			0.15	0.171	81.0	97.0	0.077	43.16	53.0	0.105	21.11	112.0	0.371	1.76	13.0	79.7	-1.06	146.9	0.258
			0.3	0.059	87.0	107.0	0.038	20.02	52.0	0.039	16.47	142.0	0.484	1.28	38.0	--	none	165.9	0.188